Lifetime measurements and evidence for triaxial nuclear shapes in ^{127}Cs

S. Aydin,[1] M. Ionescu-Bujor,[2] N. Mărginean,[2] C. Costache,[2] D. Bucurescu,[2] N. Florea,[2] T. Glodariu,[2,*] A. Ionescu,[2,3] A. Iordăchescu,[2] R. Mărginean,[2] C. Mihai,[2] R. E. Mihai,[2] A. Mitu,[2] A. Negret,[2] C. R. Niţă,[2] A. Olăcel,[2] S. Pascu,[2] L. Stroe,[2] R. Suvăilă,[2] S. Toma,[2] and A. Turturică[2]

[1]*Department of Natural and Mathematical Sciences, Faculty of Engineering, Tarsus University, 33480, Mersin, Turkey*
[2]*Horia Hulubei National Institute of Physics and Nuclear Engineering, 077125 Bucharest-Măgurele, Romania*
[3]*Faculty of Physics, University of Bucharest, 077125 Bucharest-Măgurele, Romania*

(Received 16 June 2021; revised 26 August 2021; accepted 2 November 2021; published 16 November 2021)

Rotational bands built on single quasiproton excitations in ^{127}Cs have been investigated using the ^{121}Sb(^{12}C, $\alpha 2n$) reaction and the ROSPHERE detector array at IFIN-HH, Bucharest. The lifetimes in the yrast negative-parity band based on the proton in $h_{11/2}$ orbital have been measured by applying the Doppler-shift attenuation method. The lifetime of the $7/2^+$ 273-keV state, member of the rotational band associated with the proton $g_{7/2}$ orbital, has been determined as $\tau = 1.22(5)$ ns by the fast timing technique. The experimental data were compared with the calculations performed using the quasiparticle plus triaxial rotor model and deformation parameters ϵ_2 and γ have been derived for the positive- and negative-parity structures. Evidence for triaxial nuclear shapes in the states described by the proton $h_{11/2}$ orbital was provided by both signature splitting and $B(E2, \Delta J = 2)$ transition strengths.

DOI: 10.1103/PhysRevC.104.054309

I. INTRODUCTION

The existence of nuclei with static triaxial shapes is a topic of major interest in nuclear-structure physics. Nonaxial nuclear deformation could be induced through core polarization by valence particle in anisotropic orbitals [1]. Such is the case for nuclei in the $A \approx 130$ region, where valence protons occupy low-Ω orbitals from the bottom of the $\pi h_{11/2}$ subshell, while valence neutrons occupy high-Ω orbitals from the $\nu h_{11/2}$ subshell. In odd-A nuclei of the region, rotational bands based on orbitals of the $h_{11/2}$ subshell were systematically identified and the energy differences between their two signature components, i.e., the signature splitting, was shown to be highly sensitive to the γ shape-asymmetry parameter. In odd-N nuclei, the bands involve orbitals with high-Ω values and are expected to show vanishingly small signature splitting for prolate shapes; however, these bands exhibit unusually large values of signature splitting. By using the quasiparticle plus triaxial rotor (QTR) model [2], large values of γ in the range 20–30° were established for several odd-neutron isotopes, such as $^{123-133}$Xe [3,4], $^{127-131}$Ba [4], ^{129,131}Ce [5], and ^{133}Nd [6]. In the odd-Z nuclei, the yrast negative-parity bands involve the $\Omega = 1/2$ orbital and are expected to show large signature splitting at prolate shape. The observed staggering was described within the QTR model, and good description was obtained for large γ values in $^{125-129}$Cs [7].

In recent years, considerable effort has been devoted to investigate nuclear chirality and wobbling motion as direct evidence for triaxiality. The experimental manifestation of the intrinsic chirality is a structure of two, almost degenerate, $\Delta J = 1$ rotational bands having equal parity and linked to each other by interband γ-ray transitions [8]. Chiral doublet bands were reported for the first time in odd-odd nuclei of the $A \approx 130$ mass region, and described by the $\pi h_{11/2} \otimes \nu h^{-1}_{11/2}$ configuration [9,10]. At present, chirality is a well-established phenomenon, with a large number of chiral bands observed over many parts of the nuclear chart [11].

Wobbling bands are experimentally observed as multiple rotational bands developed on high-j orbital, connected via $\Delta J = 1$ $M1 + E2$ transitions, which exhibit a dominant $E2$ character. Evidence for the nuclear wobbling mode was found in several odd-mass nuclei of the $A \approx 160$ region [12–16]. Very recently, candidates for wobbling bands were reported in odd-mass nuclei with $A \approx 130$, namely ^{135}Pr [17,18], ^{133}La [19], and ^{127}Xe [20]. Wobbling excitations in odd-A nuclei with high-j aligned particles were theoretically treated by Hamamoto [21] and Frauendorf and Dönau [22].

Valuable information about the shape of nuclear states is provided by electromagnetic transition probabilities. The aim of the present study is to investigate the deformation parameters of excited states in ^{127}Cs through lifetime measurements. The high-spin level scheme of ^{127}Cs was investigated previously by Liang *et al.* [23]. In our experiment, spectroscopic studies of the bands associated with the $g_{7/2}$, $d_{5/2}$, $g_{9/2}$, and $h_{11/2}$ proton orbitals have been performed. Lifetimes of high-spin states were determined by applying the Doppler-shift attenuation method (DSAM), and the in-beam fast timing method was used to derive lifetimes of lower lying states. The experimental details are briefly presented in Sec. II. The experimental results including the level scheme and the lifetime measurements are presented in Sec. III, while in Sec. IV

*Deceased.

the observed properties of the one-quasiparticle structures in ^{127}Cs are interpreted within the quasiparticle plus triaxial rotor model.

II. EXPERIMENTAL PROCEDURE

The excited states of ^{127}Cs were populated via the ^{121}Sb(^{12}C, $\alpha 2n$) fusion-evaporation reaction. The ^{12}C beam with an energy of 54 MeV was supplied by the FN Tandem accelerator of the Horia Hulubei National Institute of Physics and Nuclear Engineering (IFIN-HH) in Bucharest. The target consisted of 1 mg/cm^2 isotopically enriched ^{121}Sb layer evaporated on a 50 mg/cm^2 ^{208}Pb foil. The γ-ray transitions were measured by using the ROSPHERE mixed array [24], which includes 14 high-purity germanium detectors (HPGe) and 11 $LaBr_3$(Ce) scintillator detectors. The HPGe detectors were placed in three rings at the angles of 143°, 90°, and 37° with respect to the beam axis. The $LaBr_3$(Ce) scintillators were placed in angular rings at 110°, 90°, and 70° with respect to the beam direction. Energy and efficiency calibrations were performed using a ^{152}Eu source.

In the off-line analysis, data from HPGe detectors were sorted in a symmetric γ-γ coincidence matrix and three asymmetric matrices created using the detectors in the rings at 37°, 90°, and 143° on the first axis, and all detectors on the second axis. The γ-ray intensities were derived from spectra created using the symmetric matrix, while the asymmetric matrices were used for transition multipolarity assignment. For this purpose, the γ intensities corrected for efficiencies, from spectra gated on the axis with all the detectors, were used to calculate the angular distribution from oriented nuclei ratio $R_{\rm ADO}$ defined as [25] $R_{\rm ADO} = [I_\gamma(37^\circ) + I_\gamma(143^\circ)]/2I_\gamma(90^\circ)$. In the present experimental conditions, typical $R_{\rm ADO}$ values are ≈0.8 for pure dipole stretched transitions and ≈1.4 for quadrupole stretched transitions and for dipole transitions with $\Delta J = 0$. The $\Delta J = 1$ transitions having $R_{\rm ADO}$ significantly different from 0.8 are mixed transitions of $E2/M1$ type, with $\delta < 0$ for $R_{\rm ADO} < 0.8$ and $\delta > 0$ for $R_{\rm ADO} > 0.8$.

To derive lifetimes by the Doppler-shift attenuation method, spectra were created with appropriate gates in the asymmetric matrices and the experimentally observed line shapes were analysed using the code LINESHAPE [26]. The slowing history of the ^{127}Cs recoils in the target and backing was simulated using Monte Carlo techniques and a statistical distribution was created for the projection of the recoil velocity with respect to the direction of the detected γ ray. For the description of the electronic and nuclear scattering, the Ziegler stopping powers [27,28] have been used. Extraction of lifetimes was done step by step, starting from the upper levels. At each level, the intensity balance of feeding and decaying transitions was investigated to establish the amount of side feeding from unobserved transitions. In a study devoted to lifetimes and side-feeding population of the yrast band levels in ^{131}La using the ^{122}Sn(^{14}N, $5n$) reaction [29], spin-dependent effective side-feeding times were derived, with values ranging from ≈0.13 ps at spin 21/2 to ≈0.08 ps at spin 35/2 for the contribution from quasicontinuum levels. These values for the side-feeding times were adopted in the present work. To test the validity of this choice, we performed a DSAM analysis for the $23/2^-$, $27/2^-$, and $31/2^-$ states of the yrast negative-parity band in ^{129}La, well populated in our experiment. The derived lifetimes were found in very good agreement with previously reported values [30], what gave us confidence in the adopted procedure.

Lifetimes of excited states in the nanosecond range were investigated by the fast-timing method using the array of $LaBr_3$(Ce) detectors. Following the procedure presented in detail in Ref. [31], data were sorted into $E_{\gamma 1} - E_{\gamma 2} - \Delta T$ cubes, where $E_{\gamma 1}$ and $E_{\gamma 2}$ represent the energies measured in the $LaBr_3$(Ce) detectors, while ΔT represents the time difference between the detection of the two γ rays. To clean the coincidence spectra, the cubes were created with additional conditions set in the HPGe detectors.

III. EXPERIMENTAL RESULTS

A. Single-quasiproton bands in ^{127}Cs

The high-spin level scheme of ^{127}Cs was investigated previously by Liang *et al.* [23], who reported five rotational bands associated with single-quasiproton excitations and four rotational structures built on proton-neutron three quasiparticle configurations. In the present work, the rotational bands associated with the proton $g_{7/2}$, $d_{5/2}$, $g_{9/2}$, and $h_{11/2}$ orbitals were observed to be in good agreement with Ref. [23]. The structures involving three quasiparticle configurations were much more weakly populated, and only the lowest transitions could be seen due to low statistics. The ^{127}Cs level scheme studied in the present work is shown in Fig. 1, while in Table I are given the level and transition energies, the γ-ray intensities and the $R_{\rm ADO}$ ratios. Examples of gated coincidence spectra are illustrated in Fig. 2.

On the positive-parity side, the observed lowest lying bands were associated in Ref. [23] with the favored signature of the $\pi d_{5/2}$ 1/2[420] orbital, and with the favored and unfavored signature partners of the $\pi g_{7/2}$ 3/2[422] orbital. Note that in the present study the configuration assignment for the observed bands is different from that of Ref. [23]. The band assigned previously to the 1/2[420] orbital (band 3 in Ref. [23]) is assigned now as the unfavored signature partner of the $\pi g_{7/2}$ 3/2[422] orbital. Correspondingly the structure interpreted in Ref. [23] as the unfavored component of the 3/2[422] orbital is associated with the $\pi d_{5/2}$ 1/2[420] configuration. This change in configuration assignment was suggested in recent studies devoted to band structures in ^{129}Cs [32] and ^{125}Cs [33], and is supported by the signature splitting analysis in the $g_{7/2}$ band (see Sec. III). In the present study, a new weak transition of 107.3 keV was placed between the low-lying levels at 246.1 and 139.0 keV. A mixed $M1 + E2$ character was assigned to several $\Delta J = 1$ transitions between low-spin states, based on the measured $R_{\rm ADO}$. For the 206.7-keV $7/2^+ \rightarrow 5/2^+$ transition a value $\delta = +0.28(3)$ was reported [34], supported by the $R_{\rm ADO}$(206.7 keV) = 1.32(9) derived in our study.

The $g_{9/2}$ band, consisting of dipole transitions and weak crossover quadrupole transitions, was associated in Ref. [23] with the $\pi g_{9/2}$ 9/2 [404] proton-hole orbital from below the

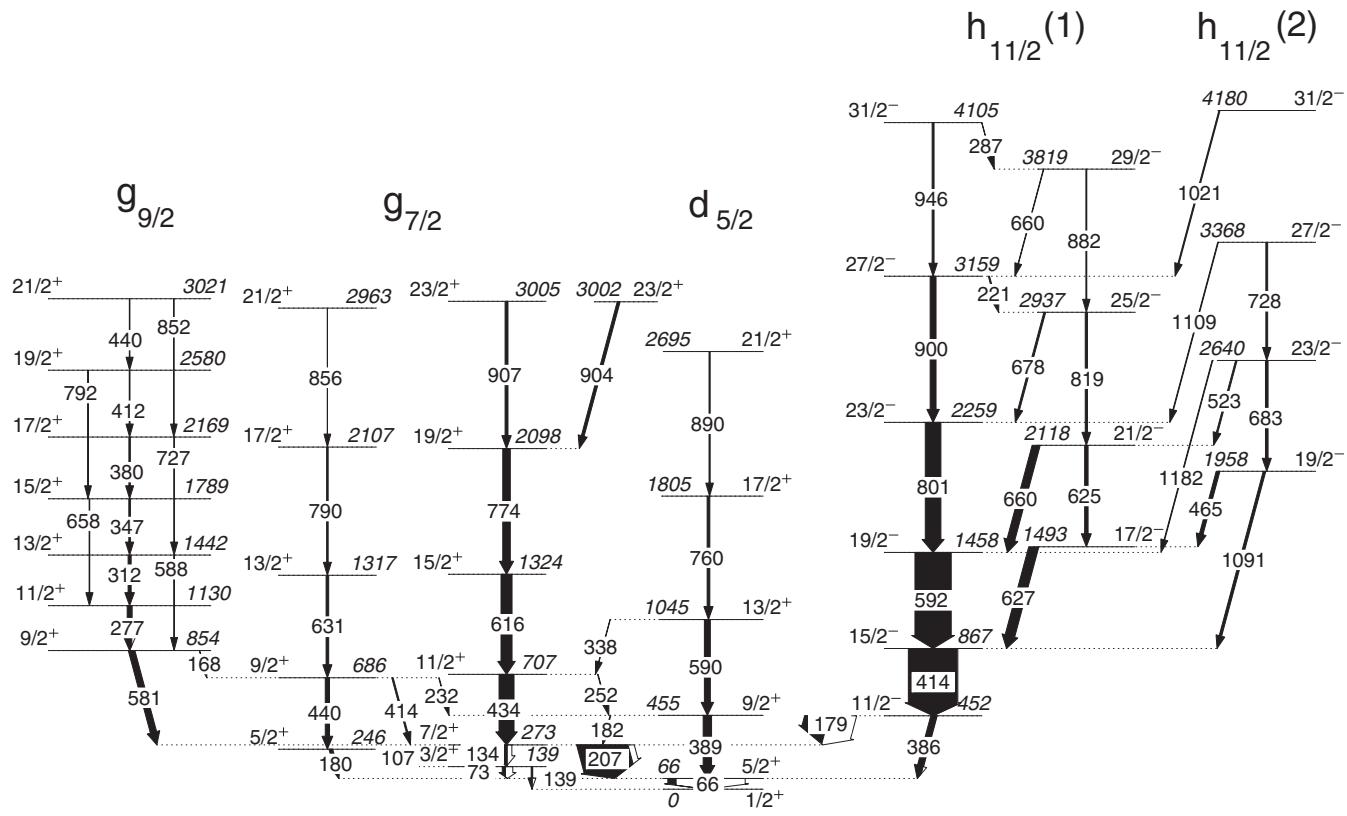

FIG. 1. Partial level scheme of ^{127}Cs investigated in the present work. The transition energies are given in keV and the widths of the arrows indicate their relative intensities.

$Z = 50$ shell closure. The R_{ADO} values of the 581, 277, 312, 347, and 380 keV $\Delta J = 1$ transitions indicate mixed $M1 + E2$ character, with positive mixing ratios (see Table I). This is in agreement with mixing ratios $\delta = +0.19(2)$, $+0.11(6)$, and $+0.11(1)$ derived for the 581-, 277-, and 347-keV transitions, respectively, in Ref. [23].

The negative-parity band $h_{11/2}(1)$ was associated in Ref. [23] with the 1/2[550] orbit, the two $\Delta J = 2$ sequences corresponding to the favored and unfavored signature partners. The states of the unfavored signature branch decay toward the states of the favored signature branch by intense $\Delta J = 1$ transitions of mixed $M1 + E2$ character. Mixing ratios δ with values of $-0.70(5)$ and $-1.1(8)$, were reported in Ref. [23] for the $21/2^- \rightarrow 19/2^-$ and $25/2^- \rightarrow 23/2^-$ transitions, respectively. The R_{ADO} ratios derived in our study for these two transitions, $R_{\mathrm{ADO}}(659.7\ \mathrm{keV}) = 0.45(10)$ and $R_{\mathrm{ADO}}(678.0\ \mathrm{keV}) = 0.38(9)$, support the assigned mixing ratios. A mixing ratio $\delta = +0.28(3)$ was reported in Ref. [23] for the 220.8-keV, $27/2^- \rightarrow 25/2^-$ transition; however, we assigned it as a pure dipole transition, based on the measured $R_{\mathrm{ADO}}(220.8\ \mathrm{keV}) = 0.75(9)$.

The second negative-parity structure described by the $h_{11/2}$ orbital was observed up to spin $31/2^-$. It is a $\Delta J = 2$ band showing at each member a significant $E2$ branch to the favored signature states of the $h_{11/2}(1)$ band. The first two states decay also by $\Delta J = 1$ mixed $M1 + E2$ transitions to the unfavored signature members of band $h_{11/2}(1)$. The measured R_{ADO} of the 465- and 523-keV transitions, 0.60(4) and 0.39(4), respectively, support the large negative mixing ratios $-0.84(28)$ and $-0.9(3)$ reported in Ref. [23].

B. Lifetimes of the high-spin negative-parity states

In the present work, the lifetimes of the high-spin states of ^{127}Cs have been investigated by applying the Doppler-shift attenuation method. For this purpose, spectra have been created from the asymmetric matrices with narrow gates on the fully stopped transitions at the bottom of the bands. In the case of the negative-parity band $h_{11/2}(1)$, gates were set on the intense 414- and 592-keV transitions at the bottom of the band, and lineshapes were analysed for de-exciting transitions of the states with $J^\pi = 21/2^-$ to $31/2^-$. Due to the much lower statistics, no DSAM analysis could be done for the other rotational bands in ^{127}Cs.

The experimental line shapes and the corresponding fits are illustrated in Figs. 3 and 4. The derived lifetimes for the $23/2^-$, $27/2^-$, and $31/2^-$ states of the favored signature, and for the $21/2^-$, $25/2^-$, and $29/2^-$ states of the unfavored signature, are collected in Table II.

C. Lifetime of the 272.9-keV $7/2^+$ state

The lifetime of the $7/2^+$ state at 272.9-keV excitation energy, member of the favored signature band with the $\pi g_{7/2}$ configuration, was measured by applying the fast-timing

TABLE I. Energies E_i of the levels in the rotational bands of ^{127}Cs associated with the proton excitation in the $g_{7/2}$, $d_{5/2}$, $g_{9/2}$, and $h_{11/2}$ orbitals, as well as transition energies E_γ, spins and parities of the initial and final states J_i^π and J_f^π, γ-ray intensities I_γ, ADO ratios, and multipolarities.

E_i (keV)	E_γ (keV)	J_i^π	J_f^π	I_γ	R_{ADO}	Multipolarity
$\pi g_{7/2}$ band						
139.0	72.9(1)	$3/2^+$	$5/2^+$	>6.0[c]		
	139.0(2)		$1/2^+$	>2.6[c]	0.67(15)	$M1$
246.1	107.3(2)	$5/2^+$	$3/2^+$	0.7(2)		
	180.0(2)		$5/2^+$	6.4(2)	1.35(15)	$M1$
272.9	133.9(2)	$7/2^+$	$3/2^+$	14(1)	1.48(19)	$E2$
	206.7(2)		$5/2^+$	102(3)	1.32(9)	$M1+E2$
686.4	231.6(3)	$9/2^+$	$9/2^+$	1.0(2)	1.49(29)	$M1$
	413.5(3)		$7/2^+$	2.8(5)	1.30(15)	$M1+E2$
	440.3(2)		$5/2^+$	8.6(3)	1.36(15)	$E2$
707.3	252.3(2)	$11/2^+$	$9/2^+$	1.1(3)	1.12(22)	$M1+E2$
	434.4(2)		$7/2^+$	30.4(9)	1.44(9)	$E2$
1317.4	631.0(3)	$13/2^+$	$9/2^+$	5.3(2)	1.24(18)	$E2$
1323.7	616.4(3)	$15/2^+$	$11/2^+$	22.5(7)	1.33(8)	$E2$
2097.7	774.0(3)	$19/2^+$	$15/2^+$	15.4(4)	1.31(11)	$E2$
2107.1	789.7(3)	$17/2^+$	$13/2^+$	3.1(2)	1.25(17)	$E2$
2962.9	855.8(4)	$21/2^+$	$17/2^+$	0.5(2)	1.34(19)	$E2$
3001.9	904.2(4)	$23/2^+$	$19/2^+$	5.7(3)	1.35(12)	$E2$
3004.7	907.0(4)	$23/2^+$	$19/2^+$	5.9(3)	1.28(14)	$E2$
$\pi d_{5/2}$ band						
66.1[a]	66.1(2)	$5/2^+$	$1/2^+$	>18.4[d]		
454.8	181.8(3)	$9/2^+$	$7/2^+$	1.2(2)	0.71(18)	$M1$
	388.7(3)		$5/2^+$	16.9(7)	1.42(8)	$E2$
1044.8	337.6(9)	$13/2^+$	$11/2^+$	0.8(2)		
	590.0(3)		$9/2^+$	12.1(6)	1.29(7)	$E2$
1805.0	760.2(4)	$17/2^+$	$13/2^+$	5.5(9)	1.35(8)	$E2$
2695.4	890.4(5)	$21/2^+$	$17/2^+$	2.3(5)	1.25(12)	$E2$
$\pi g_{9/2}$ band						
853.9	167.5(3)	$9/2^+$	$9/2^+$	0.8(2)		
	581.0(2)		$7/2^+$	13(1)	1.07(6)	$M1+E2$
1130.4	276.5(2)	$11/2^+$	$9/2^+$	9.5(6)	1.38(9)	$M1+E2$
1442.0	311.6(2)	$13/2^+$	$11/2^+$	6.0(4)	1.11(7)	$M1+E2$
	588.2(4)		$9/2^+$	0.8(2)	1.37(17)	$E2$
1788.6	346.6(3)	$15/2^+$	$13/2^+$	3.2(4)	1.16(8)	$M1+E2$
	658.2(4)		$11/2^+$	1.2(3)	1.37(17)	$E2$
2168.9	380.3(3)	$17/2^+$	$15/2^+$	2.9(4)	0.97(14)	$M1+E2$
	726.7(6)		$13/2^+$	1.1(3)		
2580.4	411.5(7)	$19/2^+$	$17/2^+$	1.5(5)	0.88(14)	$M1$
	791.8(7)		$15/2^+$	0.5(2)		
3020.7	440.3(6)	$21/2^+$	$19/2^+$	1.2(4)	0.86(13)	$M1$
	852(1)		$17/2^+$	0.4(2)		
$\pi h_{11/2}(1)$ band						
452.2[b]	179.3(3)	$11/2^-$	$7/2^+$	49(3)		$M2$[e]
	386.1(4)		$5/2^+$	12(1)		
866.5	414.3(3)	$15/2^-$	$11/2^-$	100(3)	1.53(15)	$E2$
1458.2	591.7(3)	$19/2^-$	$15/2^-$	74(5)	1.40(14)	$E2$
1493.0	626.5(4)	$17/2^-$	$15/2^-$	20(4)		
2117.9	625.0(6)	$21/2^-$	$17/2^-$	7(2)		
	659.7(3)		$19/2^-$	16(2)	0.45(10)	$M1+E2$
2259.2	801.0(4)	$23/2^-$	$19/2^-$	32(3)	1.39(14)	$E2$
2937.2	678.0(4)	$25/2^-$	$23/2^-$	3.6(4)	0.38(9)	$M1+E2$
	819.3(4)		$21/2^-$	4.5(2)	1.48(24)	$E2$
3159.2	220.8(4)	$27/2^-$	$25/2^-$	2.2(5)	0.75(9)	$M1$
	900.0(4)		$23/2^-$	12(1)	1.53(21)	$E2$

TABLE I. *(Continued.)*

E_i (keV)	E_γ (keV)	J_i^π	J_f^π	I_γ	$R_{\rm ADO}$	Multipolarity
3818.9	659.7(4)	$29/2^-$	$27/2^-$	1.0(3)		
	881.6(5)		$25/2^-$	1.8(4)	1.44(29)	$E2$
4105.4	286.5(4)	$31/2^-$	$29/2^-$	0.6(3)		
$\pi h_{11/2}(2)$ band						
	946.2(4)		$27/2^-$	3.9(8)	1.34(21)	$E2$
1957.9	464.9(2)	$19/2^-$	$17/2^-$	7.3(6)	0.60(4)	$M1+E2$
	1091.4(3)		$15/2^-$	5.1(3)	1.25(10)	$E2$
2640.4	522.5(3)	$23/2^-$	$21/2^-$	2.9(3)	0.39(4)	$M1+E2$
	682.5(3)		$19/2^-$	5.3(4)	1.41(15)	$E2$
	1182.3(5)		$19/2^-$	0.9(4)		
3368.2	727.8(3)	$27/2^-$	$23/2^-$	3.7(5)	1.31(18)	$E2$
	1109.0(7)		$23/2^-$	1.4(6)		
4179.9	1020.7(8)	$31/2^-$	$27/2^-$	2.2(6)	1.24(21)	$E2$

[a]Isomeric state with $T_{1/2} = 24.88(30)$ ns (Ref. [34]).
[b]Isomeric state with $T_{1/2} = 55(3)$ μs (Ref. [34]).
[c]Lower limit estimated using the measured intensity of the transition feeding the 139-keV level and the relative intensities of the 72.9- and 139.0-keV γ rays from Ref. [34].
[d]Lower limit estimated from the measured intensities of the transitions feeding the 66.1-keV level.
[e]From Ref. [34].

method. According to the procedure presented in Ref. [31], a $E_{\gamma 1} - E_{\gamma 2} - \Delta T$ cube was created using the $LaBr_3$(Ce) detector array, with a gate in HPGe detectors set on the 616-keV $15/2^+ \rightarrow 11/2^+$ transition of the band. To derive the lifetime

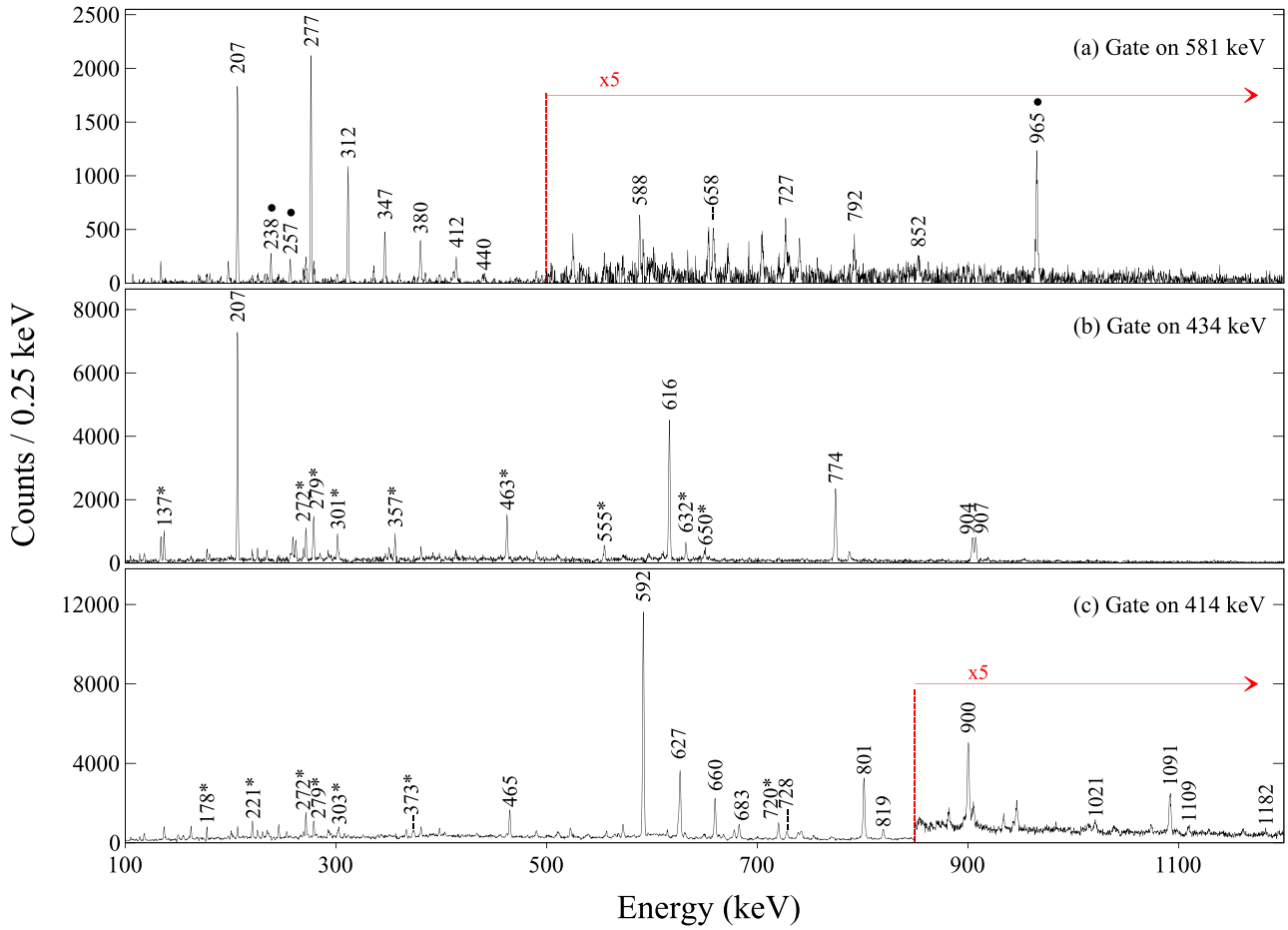

FIG. 2. Coincidence spectra from the symmetric γ-γ matrix showing transitions in the $g_{9/2}$ band (a), $g_{7/2}$ band (b), and $h_{11/2}$ band (c). Transitions denoted by a solid circle belong to ^{127}Cs (band 1 of Ref. [23]) and those denoted by a star belong to ^{130}La (Ref. [35]).

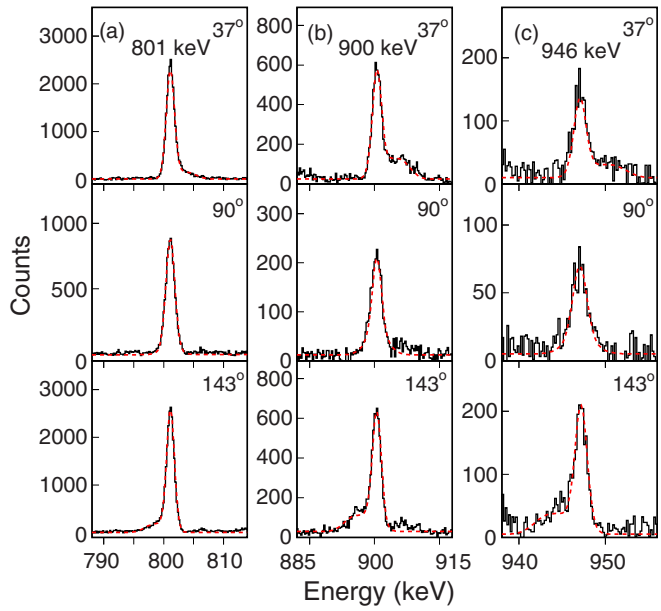

FIG. 3. Experimental and calculated lineshapes for transitions de-exciting the states in the favored branch of the negative-parity yrast band in ^{127}Cs, with $J^{\pi} = 23/2^{-}$(a), $27/2^{-}$(b), and $31/2^{-}$(c), respectively. The fitted DSAM spectra are shown in red dashed lines.

of the $7/2^{+}$ state, delayed coincidences between the feeding γ ray of 434 keV and the de-exciting 207-keV transition have been investigated. Figure 5(a) shows the $LaBr_3$(Ce) spectrum obtained by using gates on 616-keV γ rays detected in HPGe and 434-keV γ rays detected in the $LaBr_3$(Ce) detectors. In the used procedure, from the time spectrum gated by the

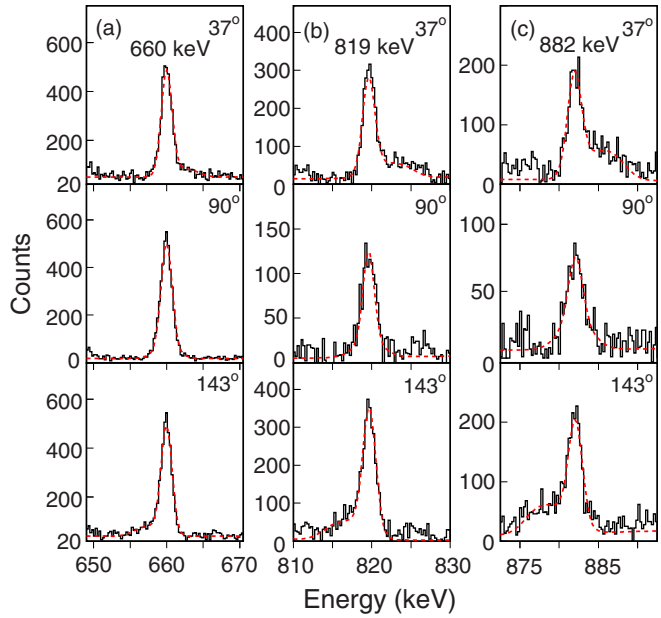

FIG. 4. Experimental and calculated lineshapes for transitions de-exciting the states in the unfavored branch of the negative-parity yrast band in ^{127}Cs, with $J^{\pi} = 21/2^{-}$(a), $25/2^{-}$(b), and $29/2^{-}$(c), respectively. The fitted DSAM spectra are shown in red dashed lines.

TABLE II. Measured level lifetimes for the $\pi h_{11/2}(1)$ band in ^{127}Cs. The quoted uncertainties include the fitting and population pattern errors, as well as the systematic errors due to the stopping power (10%) and side-feeding times (15%).

$\pi h_{11/2}$ band	E_x(keV)	J^{π}	τ (ps)
Favored signature	2259.2	$23/2^{-}$	2.55(69)
	3159.2	$27/2^{-}$	1.23(33)
	4105.4	$31/2^{-}$	1.15(30)
Unfavored signature	2117.9	$21/2^{-}$	2.45(74)
	2937.2	$25/2^{-}$	1.21(34)
	3818.9	$29/2^{-}$	0.96(27)

207-keV γ rays, a time spectrum gated by the nearby background was subtracted. As illustrated in Fig. 5(b), no prompt coincidences are present in the background subtracted time spectrum of the 207-keV γ rays. By fitting it with an exponential curve, a lifetime of $\tau = 1.22(5)$ ns has been derived for the $7/2^{+}$ state.

IV. DISCUSSION

Experimental reduced transition probabilities estimated by using the lifetimes and γ intensities determined in the present work are given in Table III. The table includes also the $5/2^{+}$ state at 66.1 keV, that is an isomeric state with a halflife

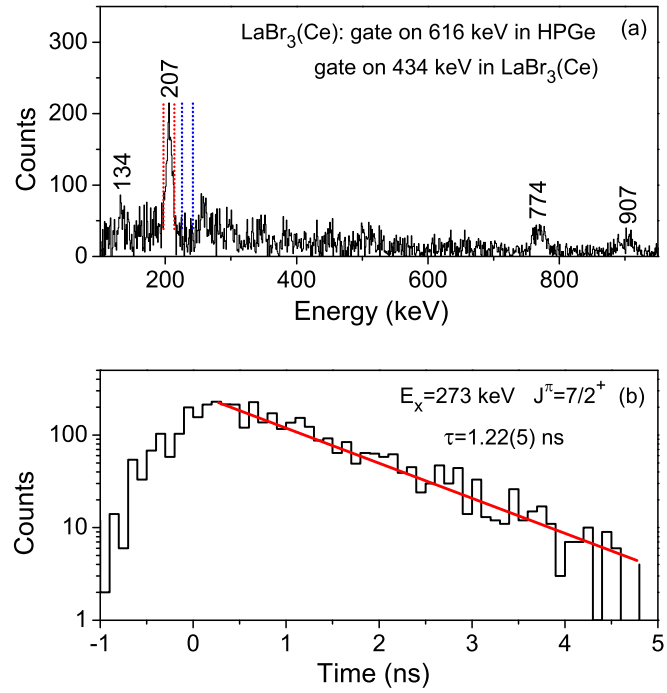

FIG. 5. (a) $LaBr_3$(Ce) energy spectrum obtained by gating on the 616-keV γ ray in HPGe detectors and on the 434-keV γ ray in $LaBr_3$(Ce) detectors. Peaks belonging to the $g_{7/2}$ favored signature band are marked by energy. (b) Experimental background-subtracted time spectrum for the 206.7-keV and the exponential fit. The gates used for the peak and background time spectra are illustrated in panel (a) with red and blue dotted lines, respectively.

TABLE III. Experimental reduced transition probabilities B(M1) and B(E2) in ^{127}Cs, derived by using the lifetimes from the present work and from Ref. [34]. In the case of the $\Delta J = 1$ transitions of 206.7, 659.7, and 678.0 keV with a mixed $M1 + E2$ character, the mixing ratio values of Ref. [34] were used. Total conversion coefficients α_T were taken from Ref. [36].

Band	E_i (keV)	$T_{1/2}$ (ps)	J_i^π	J_f^π	E_γ (keV)	δ	α_T	B(M1) (μ_N^2)	B(E2) (e^2b^2)
$\pi d_{5/2}$	66.1	24880(300)[a]	$5/2^+$	$1/2^+$	66.1(2)		8.29(15)		0.194(4)
$\pi g_{7/2}$	272.9	845(35)[b]	$7/2^+$	$5/2^+$	206.7(2)	0.28(3)	0.1218(18)	0.0036(2)	0.010(2)
				$3/2^+$	133.9(2)		0.667(10)		0.158(12)
$\pi h_{11/2}$	2259.2	1.77(48)[b]	$23/2^-$	$19/2^-$	801.0(4)		0.00283(4)		0.097(26)
Favored	3159.2	0.85(23)[b]	$27/2^-$	$25/2^-$	220.8(4)		0.1001(15)	0.66(22)	
				$23/2^-$	900.0(4)		0.00216(3)		0.094(26)
	4105.4	0.80(21)[b]	$31/2^-$	$29/2^-$	286.5(4)		0.0502(8)	0.28(15)	
				$27/2^-$	946.2(4)		0.00193(3)		0.080(22)
$\pi h_{11/2}$	2117.9	1.70(51)[b]	$21/2^-$	$19/2^-$	659.7(3)	−0.70(5)	0.00562(10)	0.038(12)	0.061(20)
Unfavored				$17/2^-$	625.0(6)		0.00519(8)		0.106(39)
	2937.2	0.84(24)[b]	$25/2^-$	$23/2^-$	678.0(4)	−1.1(8)	0.0049(8)	0.030(26)	0.114(82)
				$21/2^-$	819.3(4)		0.00268(4)		0.101(29)
	3818.9	0.67(19)[b]	$29/2^-$	$27/2^-$	659.7(4)		0.00615(9)	0.073(27)	
				$25/2^-$	881.6(5)		0.00227(4)		0.102(32)

[a]Reference [34].
[b]Present work.

$T_{1/2} = 24.88(30)$ ns [34]. Total conversion coefficients were taken from Ref. [36]. In the case of the $\Delta J = 1$ transitions of 206.7, 659.7, and 678.0 keV with a mixed $M1 + E2$ character, the mixing ratios given in Ref. [34] were used. The other $\Delta J = 1$ transitions were considered pure $M1$.

In the present study, we performed calculations of the positive- and negative-parity structures in ^{127}Cs using the QTR model of Ref. [2]. The single-particle energies are calculated in a modified oscillator (Nilsson) potential with the κ and μ parameters taken from Ref. [37]. Pairing was treated in the usual way within the BCS approximation with standard value for the pairing strength [38]. The core moments of inertia were calculated in such a way that the experimental energy of the 2^+ state of the even-even ^{128}Ba nucleus was reproduced. In evaluating the $B(M1)$ transition strengths, an effective g_s factor of $0.7g_s^{\rm free}$ has been used and g_R has been taken as Z/A. Quadrupole moments of the core were calculated macroscopically. For the positive-parity state calculations, all the $N = 4$ single-particle orbitals were included, while for the negative-parity state calculations all orbitals of the $h_{11/2}$ state have been considered. The deformation parameters ϵ_2 and γ were varied to obtain the best description of both the reduced transition probabilities $B(E2)$ and the signature splitting $S(J)$, calculated with the expression (Ref. [3])

$$S(J) = \frac{E(J) - E(J-1)}{E(J) - E(J-2)} \frac{J(J+1) - (J-2)(J-1)}{J(J+1) - J(J-1)} - 1. \quad (1)$$

The calculations revealed that by changing ϵ_2 there was a significant change in $B(E2)$ values, but practically no change in the signature splitting.

The QTR model calculations of the positive-parity states, performed for $\gamma = 0^\circ$, reproduce well the experimentally observed sequences of states, with the $1/2^+$ ground state described by a dominant 1/2[420] configuration from the $d_{5/2}$ orbital. The structure of the $g_{7/2}$ band involves predominant components from the $g_{7/2}$ orbital with some mixing from the $d_{5/2}$ orbital.

As seen in Fig. 6, the experimental signature splitting values $S(J)$ for the $g_{7/2}$ band are very well reproduced for $\gamma = 0^\circ$. The good description with the QTR model gives support to the adopted configuration assignment for the low-lying $d_{5/2}$ and $g_{7/2}$ bands, that is different from that of Ref. [23]. With the inclusion of a nonzero γ parameter, the description of the low-lying states is worse. In particular, for small values of the triaxial parameter ($1^\circ \leqslant \gamma \leqslant 13^\circ$) the spin of the ground state is predicted $3/2^+$ instead of $1/2^+$. For all γ values, at low spins the experimental $S(J)$ are not reproduced by the calculated ones (see Fig. 6 for an illustrative example).

By comparing the experimental transition probabilities $B(E2)(5/2^+ \to 1/2^+)$ and $B(E2)(7/2^+ \to 3/2^+)$ with QTR estimates in the $d_{5/2}$ and $g_{7/2}$ bands (see Fig. 7), a quadrupole

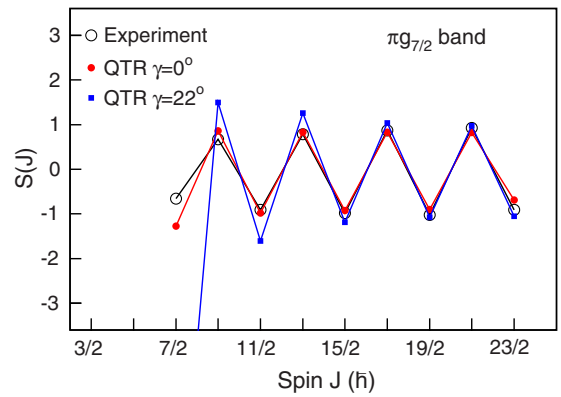

FIG. 6. Experimental signature splitting $S(J)$ for the band based on the $g_{7/2}$ proton orbital (empty black circle) compared with the theoretical values calculated for a quadrupole deformation $\epsilon_2 = 0.18$ and $\gamma = 0^o$ (red full circle) and $\gamma = 22^o$ (blue full square).

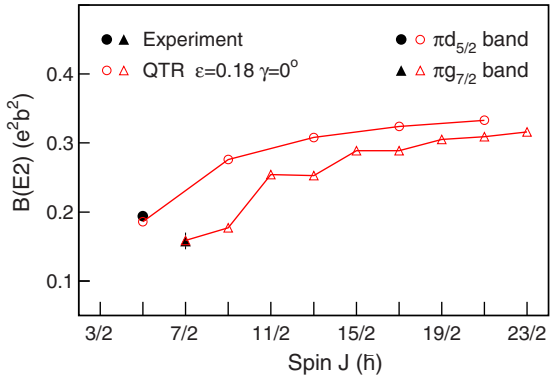

FIG. 7. Experimental transition probabilities $B(E2)(5/2^+ \rightarrow 1/2^+)$ (full black circle) and $B(E2)(7/2^+ \rightarrow 3/2^+)$ (full black triangle) compared with QTR model calculations for the proton $d_{5/2}$ band (red empty circle) and $g_{7/2}$ band (red empty triangle)

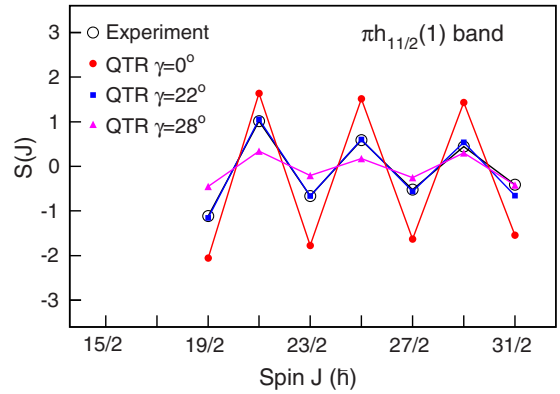

FIG. 8. Experimental signature splitting $S(J)$ for the band based on the proton $h_{11/2}$ orbital (empty black circle) compared with the theoretical values calculated for a quadrupole deformation $\epsilon_2 = 0.11$ and $\gamma = 0^o$ (red full circle), $\gamma = 22^o$ (blue full square), and $\gamma = 28^o$ (magenta full triangle).

deformation parameter $\epsilon_2 = 0.18$ has been established for the positive-parity states in ^{127}Cs.

The energy of the $9/2^+$ state with the dominant 9/2[404] configuration from the $g_{9/2}$ orbital is predicted by the QTR model to be strongly dependent on the quadrupole deformation. For $\epsilon_2 = 0.14$ its energy is calculated at 1313 keV, while for $\epsilon_2 = 0.22$ the energy is predicted at 309 keV, below the energies of the $9/2^+$ states in the $d_{5/2}$ and $g_{7/2}$ bands. Interestingly, for the quadrupole deformation $\epsilon_2 = 0.18$ adopted on the basis of $B(E2)$ values, the calculated excitation energy of the $g_{9/2}$ bandhead is 827 keV, close to the experimental energy of 854 keV. The observed decay of this state toward members of the $g_{7/2}$ band and the lack of transitions toward the $d_{5/2}$ band is also well described by the QTR calculations, giving support to the present rearrangement of these bands.

It is worthwhile to mention that the deformation of the positive-parity states adopted on the basis of $B(E2)$ transition probabilities is in excellent agreement with the value $\epsilon_2 = 0.175$ predicted for the ^{127}Cs ground state in the macroscopic-microscopic calculations tabulated in Ref. [39].

The structure of the negative-parity states was calculated to involve a mixing of states from the $\pi h_{11/2}$ orbital. The yrast favored signature states exhibit a dominant $K = 1/2$ value, while the unfavored states have a dominant $K = 3/2$. The experimental signature splitting is compared in Fig. 8 with QTR model calculations. For $\gamma = 0^\circ$, no good fit can be obtained, as the calculated $S(J)$ values are much larger compared to the experimental ones. The calculated staggering is found to decrease by using a triaxial parameter different from zero. As seen in Fig. 8, the best description is obtained for a triaxial parameter $\gamma = 22^\circ$. This is similar to the conclusion obtained in the study of Ref. [7].

By comparing the experimental reduced transition probabilities in the yrast negative-parity band with QTR model calculations, a deformation parameter $\epsilon_2 = 0.11$ has been determined. The experimental $B(E2)$ values are illustrated in Fig. 9 together with theoretical values calculated for this quadrupole deformation and for $\gamma = 0^o$ and $\gamma = 22^o$. An interesting feature revealed by the calculations is that for $\gamma = 0^\circ$ a staggering of the $B(E2)$ values between the two signature partners is predicted, the values being larger for the favored signature. No staggering is observed in the experimental data, in accordance with the calculations performed using $\gamma = 22^o$. Direct evidence for triaxiality is thus provided by the measured lifetimes in the $\pi h_{11/2}$ band. It is worthwhile to mention that lifetimes in the $\pi h_{11/2}$ band have been previously reported in ^{125,127}La [40], ^{129}La [30], ^{131}La [29] and ^{129}Cs [41]; however, in all these studies only the favored signature branch was investigated. In the present work, for the first time $B(E2)$ values were reported in both favored and unfavored signature states and this was crucial for probing the triaxial shape in the $\pi h_{11/2}$ band.

The calculated $B(M1)$ strengths for the $\Delta J = 1$ pure transitions from the $27/2^-$ and $31/2^-$ states of the favored signature branch have values of 0.49 and 0.54 μ_N^2, respectively, in rather good agreement with experimental values (see Table III). The description of the $\Delta J = 1$ mixed $M1 + E2$ transitions from unfavored to favored signature partners was less good. The calculated $B(M1)$ values are about an order of magnitude larger than the experimental ones, while the $B(E2, \Delta J = 1)$

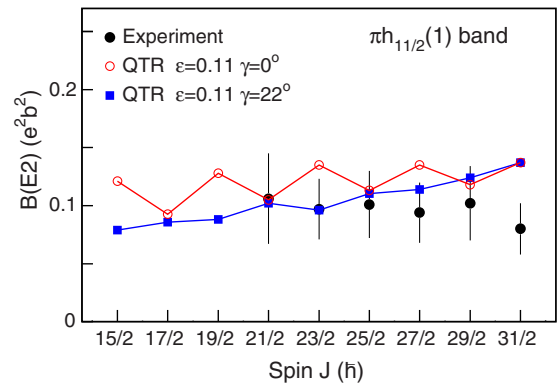

FIG. 9. Experimental transition probabilities for the yrast band based on the proton $h_{11/2}$ orbital (full black circle) compared with theoretical values calculated for a quadrupole deformation $\epsilon_2 = 0.11$ and $\gamma = 0^o$ (red open circle) and $\gamma = 22^o$ (blue full square).

strengths are predicted smaller than the experimentally derived values.

In the QTR model calculations, the yrare favored signature states have a dominant $K = 5/2$ value. For $\gamma = 0^\circ$, their energies were predicted to be more than 1 MeV higher compared to the experimental states of the $h_{11/2}(2)$ band. With the inclusion of nonzero γ values, the calculated energies are smaller. For $\gamma = 22^o$, the energy of the yrare $19/2^-$ state is calculated at 2035 keV, in accordance with the experimental value of 1958 keV. This gives additional support for triaxial shapes in the $h_{11/2}$ bands.

An interesting result of the present study is that two sets of deformation parameter values have been established, $\epsilon_2 = 0.18$, $\gamma = 0^\circ$ for the positive-parity states and $\epsilon_2 = 0.11$, $\gamma = 22^\circ$ for the negative-parity states. Core polarization effects induced by various orbitals are expected in this transitional nuclear region. The present results indicate that due to polarizing $h_{11/2}$ protons the core is soft to both the quadrupole deformation and shape asymmetry.

V. SUMMARY

The rotational bands based on one-proton excitation in ^{127}Cs were investigated via the ^{121}Sb(^{12}C, $\alpha 2n$) fusion-evaporation reaction using the ROSPHERE mixed array. Lifetimes of six states in the negative-parity band based on the $\pi h_{11/2}$ orbital have been measured by applying the Doppler-shift attenuation method. The lifetime of the $7/2^+$ 273-keV state, member of the rotational band based on the $\pi g_{7/2}$ orbital, was derived by using the in-beam fast timing method. Theoretical investigations were carried out for both positive- and negative-parity structures using the quasiparticle plus triaxial rotor model. The observed properties of the positive-parity $g_{7/2}$, $d_{5/2}$, and $g_{9/2}$ bands were described in a consistent way with the deformation parameters $\epsilon_2 = 0.18$ and $\gamma = 0^\circ$. For axially symmetric shapes, the $B(E2)$ reduced transition probabilities in the band based on the $h_{11/2}$ orbital are predicted to exhibit a staggering between the favored and unfavored branches, in disagreement with the experimental $B(E2)$ values that show a smooth dependence on spin. By comparing the experimental signature splitting and transition strength values in the $h_{11/2}$ band with theoretical calculations, the deformation parameters $\epsilon_2 = 0.11$ and $\gamma = 22^\circ$ were established. The present results provide further evidence for triaxial nuclear shape in the states involving the proton $h_{11/2}$ orbital of ^{127}Cs.

ACKNOWLEDGMENTS

Authors are thankful to the FN Tandem staff of the Horia Hulubei National Institute of Physics and Nuclear Engineering for the good quality beam. This work was supported by the Ministry of Research, Innovation, and Digitization, Romania, Contract No. PN-19-06-01-02, and by a grant of the Ministry of Research, Innovation, and Digitization, CNCS/CCCDI-UEFISCDI, Romania, Project No. PN-III-P1-1.1-TE-2019-0337.

[1] S. Frauendorf and F. R. May, Phys. Lett. B **125**, 245 (1983).
[2] S. E. Larsson, G. Leander, and I. Ragnarsson, Nucl. Phys. A **307**, 189 (1978).
[3] D. Lieberz, A. Gelberg, P. von Brentano, I. Ragnarsson, and P. B. Semmes, Phys. Lett. B **282**, 7 (1992).
[4] A. Gelberg, D. Lieberz, P. von Brentano, I. Ragnarsson, P. B. Semmes, and I. Wiedenhóver, Nucl. Phys. A **557**, 439 (1993).
[5] M. Ionescu-Bujor, A. Iordăchescu, F. Brandolini, M. De Poli, N. H. Medina, P. Pavan, M. N. Rao, and C. Rossi Alvarez, Nucl. Phys. A **633**, 459 (1998).
[6] D. Bazzacco, F. Brandolini, G. Falconi, S. Lunardi, N. H. Medina, P. Pavan, C. Rossi Alvarez, G. de Angelis, D. De Acuna, M. De Poli, D. R. Napoli, J. Rico, D. Bucurescu, M. Ionescu-Bujor, and C. A. Ur, Phys. Rev. C **58**, 2002 (1998).
[7] O. Vogel, A. Gelberg, R. V. Jolos, and P. von Brentano, Nucl. Phys. A **576**, 109 (1994).
[8] S. Frauendorf and J. Meng, Nucl. Phys. A **617**, 131 (1997).
[9] K. Starosta, T. Koike, C. J. Chiara, D. B. Fossan, D. R. LaFosse, A. A. Hecht, C. W. Beausang, M. A. Caprio, J. R. Cooper, R. Krucken, J. R. Novak, N.V. Zamfir, K. E. Zyromski, D. J. Hartley, D. Balabanski, J. Y. Zhang, S. Frauendorf, and V. I. Dimitrov, Phys. Rev. Lett. **86**, 971 (2001).
[10] T. Koike, K. Starosta, C. J. Chiara, D. B. Fossan, and D. R. LaFosse, Phys. Rev. C **63**, 061304(R) (2001).
[11] B. W. Xiong and Y. Y. Wang, At. Data Nucl. Data Tables **125**, 193 (2019).
[12] S. W. Odegard, G. B. Hagemann, D. R. Jensen, M. Bergstrom, B. Herskind, G. Sletten, S. Tormanen, J. N. Wilson, P. O. Tjom, I. Hamamoto, K. Spohr, H. Hubel, A. Gorgen, G. Schonwasser, A. Bracco, S. Leoni, A. Maj, C. M. Petrache, P. Bednarczyk, and D. Curien, Phys. Rev. Lett. **86**, 5866 (2001).
[13] G. Schönwaßer, H. Hübel, G. B. Hagemann, P. Bednarczyk, G. Benzoni, A. Bracco, P. Bringel, R. Chapman, D. Curien, J. Domscheit, B. Herskind, D. R. Jensen, S. Leoni, G. Lo Bianco, W. C. Ma, A. Maj, A. Neußer, S. W. Ødegård, C. M. Petrache, D. Roß bach, H. Ryde, K. H. Spohr, and A. K. Singh, Phys. Lett. B **552**, 9 (2003).
[14] H. Amro, W. C. Ma, G. B. Hagemann, R. M. Diamond, J. Domscheit, P. Fallon, A. Görgen, B. Herskind, H. Hübel, D. R. Jensen, Y. Li, A. O. Macchiavelli, D. Roux, G. Sletten, J. Thompson, D. Ward, I. Wiedenhöver, J. N. Wilson, and J. A. Winger, Phys. Lett. B **553**, 197 (2003).
[15] P. Bringel, G. B. Hagemann, H. Hübel, A. Al-khatib, P. Bednarczyk, A. Bürger, D. Curien, G. Gangopadhyay, B. Herskind, D. R. Jensen, D. T. Joss, T. Kröll, G. Lo Bianco, S. Lunardi, W. C. Ma, N. Nenoff, A. Neuß er-Neffgen, C. M. Petrache, G. Schönwasser, J. Simpson, A. K. Singh, N. Singh, and G. Sletten, Eur. Phys. J. A **24**, 167 (2005).
[16] D. J. Hartley, R. V. F. Janssens, L. L. Riedinger, M. A. Riley, A. Aguilar, M. P. Carpenter, C. J. Chiara, P. Chowdhury, I. G. Darby, U. Garg, Q. A. Ijaz, F. G. Kondev, S. Lakshmi, T. Lauritsen, A. Ludington, W. C. Ma, E. A. McCutchan, S.

Mukhopadhyay, R. Pifer, E. P. Seyfried *et al.*, Phys. Rev. C **80**, 041304(R) (2009).

[17] J. T. Matta, U. Garg, W. Li, S. Frauendorf, A. D. Ayangeakaa, D. Patel, K. W. Schlax, R. Palit, S. Saha, J. Sethi, T. Trivedi, S. S. Ghugre, R. Raut, A. K. Sinha, R. V. F. Janssens, S. Zhu, M. P. Carpenter, T. Lauritsen, D. Seweryniak, C. J. Chiara, F. G. Kondev, D. J. Hartley, C. M. Petrache, S. Mukhopadhyay, D. V. Lakshmi, M. K. Raju, P. V. Madhusudhana Rao, S. K. Tandel, S. Ray, and F. Dönau, Phys. Rev. Lett. **114**, 082501 (2015).

[18] N. Sensharma, U. Garg, S. Zhu, A. D. Ayangeakaa, S. Frauendorf, W. Li, G. H. Bhat, J. A. Sheikh, M. P. Carpenter, Q. B. Chen, J. L. Cozzi, S. S. Ghugre, Y. K. Gupta, D. J. Hartley, K. B. Howard, R. V. F. Janssens, F. G. Kondev, T. C. McMaken, R. Palit, J. Sethi *et al.*, Phys. Lett. B **792**, 170 (2019).

[19] S. Biswas, R. Palit, S. Frauendorf, U. Garg, W. Li, G. H. Bhat, J. A. Sheikh, J. Sethi, S. Saha, P. Singh, D. Choudhury, J. T. Matta, A. D. Ayangeakaa, W. A. Dar, V. Singh, and S. Sihotra, Eur. Phys. J. A **55**, 159 (2019).

[20] S. Chakraborty, H. P. Sharma, S. S. Tiwary, C. Majumder, A. K. Gupta, P. Banerjee, S. Ganguly, S. Rai, Pragati, Mayank, S. Kumar, A. Kumar, R. Palit, S. S. Bhattacharjee, R. P. Singh, and S. Muralithar, Phys. Lett. B **811**, 135854 (2020).

[21] I. Hamamoto, Phys. Rev. C **65**, 044305 (2002).

[22] S. Frauendorf and F. Dönau, Phys. Rev. C **89**, 014322 (2014).

[23] Y. Liang, R. Ma, E. S. Paul, N. Xu, D. B. Fossan, and R. A. Wyss, Phys. Rev. C **42**, 890 (1990).

[24] D. Bucurescu, I. Căta-Danil, G. Ciocan, C. Costache, D. Deleanu, R. Dima, D. Filipescu, N. Florea, D. G. Ghiţă, T. Glodariu, M. Ivaşcu, R. Lică, N. Mărginean, R. Mărginean, C. Mihai, A. Negret, C. R. Niţă, A. Olăcel, S. Pascu, T. Sava, L. Stroe, A. Şerban, R. Şuvăilă, S. Toma, N. V. Zamfir, G. Căta-Danil, I. Gheorghe, I. O. Mitu, G. Suliman, C. A. Ur, T. Braunroth, A. Dewald, C. Fransen, A. M. Bruce, Zs. Podolyak, P. H. Regan, and O. J. Roberts, Nucl. Instrum. Methods Phys. Res., Sect. A **837**, 1 (2016).

[25] M. Piiparinen, A. Ataç, J. Blomqvist, G. B. Hagemann, B. Herskind, R. Julin, S. Juutinen, A. Lampinen, J. Nyberg, G. Sletten, P. Tikkanen, S. Törmänen, A. Virtanen, and R. Wyss, Nucl. Phys. A **605**, 191 (1996).

[26] J. C. Wells and N. R. Johnson, Report No. ORNL-6689, 1991, p. 44 (unpublished).

[27] J. F. Ziegler, *The Stopping and Range of Ions in Matter* (Pergamon Press, New York, 1980), Vols. 3 and 5.

[28] J. F. Ziegler, J. P. Biersack, and V. Littmark, *The Stopping Power and Range of Ions in Solid* (Pergamon Press, New York, 1985), Vol. 1.

[29] E. Grodner, A. A. Pasternak, Ch. Droste, T. Morek, J. Srebrny, J. Kownacki, W. Plociennik, A. A. Wasilewski, M. Kowalczyk, M. Kisielinski, R. Kaczarowski, E. Ruchowska, A. Kordyasz, and M. Wolinska, Eur. Phys. J. A **27**, 325 (2006).

[30] I. Sankowska, Ch. Droste, E. Grodner, T. Morek, J. Srebrny, A. A. Pasternak, J. Kownacki, P. Napiorkowski, S. G. Rohozinski, M. Kowalczyk, M. Kisielinski, R. Kaczarowski, and E. Ruchowska, Eur. Phys. J. A **37**, 169 (2008).

[31] N. Mărginean, D. L. Balabanski, D. Bucurescu, S. Lalkovski, L. Atanasova, G. Căta-Danil, I. Căta-Danil, J. M. Daugas, D. Deleanu, P. Detistov, G. Deyanova, D. Filipescu, G. Georgiev, D. Ghiţă, K. A. Gladnishki, R. Lozeva, T. Glodariu, M. Ivaşcu, S. Kisyov, C. Mihai, R. Mărginean, A. Negret, S. Pascu, D. Radulov, T. Sava, L. Stroe, G. Suliman, and N. V. Zamfir, Eur. Phys. J. A **46**, 329 (2010).

[32] S. Sihotra, K. Singh, S. S. Malik, J. Goswamy, R. Palit, Z. Naik, D. Mehta, N. Singh, R. Kumar, R. P. Singh, and S. Muralithar, Phys. Rev. C **79**, 044317 (2009).

[33] J. Sun, Y.-J. Ma, T. Komatsubara, K. Furuno, Y.-H. Zhang, W.-P. Zhou, S.-Y. Wang, X.-Y. Hu, H. Guo, J.-Q. Wang, and Y.-Z. Liu, Phys. Rev. C **93**, 064301 (2016).

[34] A. Hashizume, Nucl. Data Sheets **112**, 1647 (2011).

[35] M. Ionescu-Bujor, S. Aydin, A. Iordăchescu, N. Mărginean, S. Pascu, D. Bucurescu, C. Costache, N. Florea, T. Glodariu, A. Ionescu, R. Mărginean, C. Mihai, R. E. Mihai, A. Mitu, A. Negret, C. R. Niţă, A. Olăcel, B. Saygı, L. Stroe, R. Suvăilă, S. Toma, and A. Turturică, Phys. Rev. C **102**, 044311 (2020).

[36] T. Kibédi, T. W. Burrows, M. B. Trzhaskovskaya, P. M. Davidson, and C. W. Nestor Jr., Nucl. Instrum. Methods Phys. Res. Sect. A **589**, 202 (2008).

[37] J.-Y. Zhang, N. Xu, D. B. Fossan, Y. Liang, R. Ma, and E. S. Paul, Phys. Rev. C **39**, 714 (1989).

[38] S. G. Nilsson, C. F. Tsang, A. Sobiczewski, Z. Szymański, S. Wycech, C. Gustafsson, I.-L. Lamm, P. Möller, and B. Nilsson, Nucl. Phys. A **131**, 1 (1969).

[39] P. Möller, J. R. Nix, W. D. Myers, and W. J. Swiatecki, At. Data Nucl. Data Tables **59**, 185 (1995).

[40] K. Starosta, C. Droste, T. Morek, J. Srebrny, D. B. Fossan, S. Gundel, J. M. Sears, I. Thorslund, P. Vaska, M. P. Waring, S. G. Rohozinski, W. Satula, U. Garg, S. Naguleswaran, and J. C. Walpe, Phys. Rev. C **55**, 2794 (1997).

[41] U. Lamani, P. Das, B. Bhujang, and V. Pasi, Nucl. Phys. A **1014**, 122220 (2021).